Neutron Reflectivity Determination of Buried Electroactive Interface Structure: PBT/PPy and PBT/PXV Bilayers

A. Robert Hillman,*,† Paul M. Saville,† Andrew Glidle,‡ Robert M. Richardson,§ Stephen J. Roser,|| Marcus J. Swann,‡ and John R. P. Webster⊥

Contribution from the Department of Chemistry, University of Leicester, Leicester LE1 7RH, U.K., Bioelectronics, Glasgow University, Glasgow G12 8QQ, U.K., School of Chemistry, University of Bristol, Bristol BS8 1TS, U.K., School of Chemistry, University of Bath, Bath BA2 7AY, U.K., and ISIS Facility, Rutherford Appleton Laboratory, Didcot, Oxfordshire OX11 0QX, U.K.

Received January 28, 1997. Revised Manuscript Received October 14, 1998

Abstract: Structure−property correlations of two electroactive polymer bilayers fabricated by different methods are investigated using neutron reflectivity to probe the buried polymer/polymer interfaces. Both bilayers utilize electropolymerized poly(2,2′-bithiophene) as an inner, mediating layer, while the outer layer consists of either electropolymerized polypyrrole or electroprecipitated polyxylylviologen, respectively. These devices have very different current−potential behaviors, which neutron reflectivity shows is a consequence of the fabrication method and the resulting polymer/polymer interfacial structure. The polybithiophene/polypyrrole film is found to be of composite structure while polybithiophene/polyxylylviologen forms a film comprised of segregated polymer layers.

Introduction

In this paper, for the first time, we use neutron reflectivity to directly determine the spatial distributions of individual polymers in multicomponent modified electrodes. The key issue is that, in such systems, current−voltage characteristics are primarily determined by spatial distributions of material. Determination of the structure of buried interfaces between the component polymers is central to establishment of structure−property relationships and, thereby, to rational design of the interfacial architecture of modified electrochemical interfaces. The methodology described here offers this prospect.

Bilayers and Composites. One of the key factors which determines the performance of a polymer modified electrode is its structure. The process of ion transport through the polymer matrix, required for the preservation of electroneutrality, occurs at a rate which depends on the film density. Thus, comprehending the structure−property correlations of an electrochemical system is a necessary step in understanding the many factors which influence its behavior.

Electroactive polymer films are potential candidates for use in many applications attracting enormous research interest over the past decade.[1] An interesting line of enquiry is the use of more than one polymer component. At one extreme is the addition of an electroinactive polymer to yield a composite of improved mechanical properties, for example polypyrrole/poly(ethylene oxide) composites for batteries.[2] By sequential or simultaneous electropolymerization of monomers, it is possible to exercise some control over whether two-component films comprise copolymers or segregated layers.[3] The latter structures, electroactive bilayers, were first explored by Murray.[4] Direct electronic communication between the outer layer and the underlying electrode is prohibited, and outer layer redox state changes can only be mediated by the inner layer. The unidirectional character of this interfacial mediated reaction suggests applications in electronic devices, such as diodes.[5,6] Extension to electroactive trilayers offers interesting charge separation possibilities.[7]

Analysis of the kinetic and diffusional processes involved in bilayer redox switching showed that inner layer charge transport would most commonly be rate limiting,[8,9] with interfacial charge transfer at the polymer/polymer interface as the most likely alternative. The limitation of this, our own[10,11] and other[8,9] early work on conducting polymer bilayers, was its reliance on current−voltage curve analysis. At best, the determination of overall charge injection rates is a very indirect structural probe. Some assistance with the distribution of electronic charge was provided by visible transmission spectroscopy.[12,13] Gravimetric (electrochemical quartz crystal microbalance) information on the associated ion and solvent transport[14] completed the picture of the transport of mobile species.

* To whom correspondence should be addressed (e-mail: arh7@le.ac.uk).
† University of Leicester.
‡ Glasgow University.
§ University of Bristol.
|| University of Bath.
⊥ Rutherford Appleton Laboratory.

(1) Hillman, A. R. In *Electrochemical Technology of Polymers*; Linford, R., Ed.; Elsevier: London, 1987; p 103.
(2) Novak, P.; Inganas, O. *J. Electrochem. Soc.* **1988**, *135*, 2485.
(3) William, K. W.; Murray, R. W. *J. Electroanal. Chem.* **1982**, *133*, 211.
(4) Abruna, H. D.; Denisevich, P.; Umana, M.; Meyer, T. J.; Murray, R. W. *J. Am. Chem. Soc.* **1981**, *103*, 1.
(5) Denisevich, P.; William, K. W.; Murray, R. W. *J. Am. Chem. Soc.* **1981**, *103*, 4727.
(6) Aizawa, M.; Shinohara, H. *Synth. Met.* **1987**, *18*, 711.
(7) Downard, A. J.; Surridge, N. A.; Meyer, T. J.; Cosnier, S.; Deronzier, A.; Moutet, J.-C. *J. Electroanal. Chem.* **1988**, *246*, 321.
(8) Leidner, C. R.; Denisevich, P.; William, K. W.; Murray, R. W. *J. Electroanal. Chem.* **1984**, *164*, 63.
(9) Pickup, P. G.; Leidner, C. R.; Denisevich, P.; Murray, R. W. *J. Electroanal. Chem.* **1984**, *164*, 39.
(10) Hillman, A. R.; Mallen, E. F. *J. Electroanal. Chem.* **1990**, *281*, 109.
(11) Hillman, A. R.; Mallen, E. F. *J. Electroanal. Chem.* **1991**, *309*, 159.
(12) Hillman, A. R.; Mallen, E. F. *Faraday Trans.* **1991**, *87*, 2209.
(13) Hillman, A. R.; Mallen, E. F. *Electrochim. Acta* **1992**, *37*, 1887.
(14) Hillman, A. R.; Glidle, A. *J. Electroanal. Chem.* **1994**, *379*, 365.

10.1021/ja970301h CCC: $15.00
Published on Web 12/01/1998

The missing element in this picture is a direct probe of the "fixed" matrix within which the mobile species move, i.e., the spatial distributions of the two polymer components. Recently, we showed how in situ neutron reflectivity measurements on single-component conducting polymer films can yield the spatial distribution of polymer with high resolution in the z-direction.[15,16] The common visualization of polymer modified electrode films as a uniform slab of material was found to be woefully inadequate. The logical extension of this work, which we now describe, is to bilayer films.

We are particularly interested in the nature of the buried polymer/polymer interface since, regardless of the rate-limiting step,[9] it is a key determinant of bilayer switching performance. If inner layer charge transport is rate limiting, it determines the minimum inner layer distance across which charge must be transported. If polymer/polymer interfacial kinetics are rate limiting, it determines the interfacial contact area for mediated charge transfer.

Neutron Reflectivity. Neutron reflectivity provides structural information in the direction (z) perpendicular to an interface, over a length scale of 1−500 nm with a resolution, in principle, of about 0.2 nm. The neutron's penetrating power and its sensitivity to isotopic composition has allowed neutron reflectivity to become a recognized technique for probing surface and interface structures ranging from insoluble monolayers at the air/water[17] interface, to polymer films,[18] to high-temperature superconductors.[19] This capability has recently been reviewed.[20] The penetrating power of the neutrons is a consequence of their weak interaction with matter. An important advantage this confers on the methodology used here (as compared to certain X-ray methods) is the absence of sample damage, even upon prolonged exposure to the neutron beam.

The basic principle of neutron reflectivity[18] is analogous to the optical case, with the reflected intensity, R, being defined by the wavelength, λ, the incident angle, θ, and the refractive indexes of the reflecting layers, n_i, in accordance with the Fresnel equations. The reflectivity can be approximated by

$$R(Q) = \frac{(4\pi Nb)^2}{Q^4}\left[\int_{-\infty}^{\infty} \frac{\partial(Nb(z))}{\partial z} e^{iQz}\, dz\right]^2 \qquad (1)$$

where Q is the momentum transfer which the neutron experiences on reflection and is a convenient parameter relating λ and θ ($Q = (4\pi \sin\theta)/\lambda$). Nb, the scattering length density (i.e., the product of the number density, N, in units of nuclei per cm^3, and the sum of the neutron scattering lengths, b, of the different nuclei present) is the major factor determining the neutron refractive index, n ($n = 1 - \lambda^2 Nb/(2 + i\beta)$). $i\beta$ is related to absorption processes, which are negligible for most nuclei. b varies from nucleus to nucleus, so changing the isotopic composition of a system changes the reflectivity. From eq 1, it is seen that the reflectivity is a function of two terms. Via the first term, R is proportional to Q^{-4}, which is the Fresnel reflectivity due to reflection from a single interface. Via the second term, R is proportional to the Fourier transform of the scattering length density profile perpendicular to the reflecting interface.

Using the Fresnel equations it is possible to directly calculate a reflectivity profile from a scattering length density profile. However, the reverse operation is not possible due to a lack of phase information. Thus, to obtain a scattering length density profile from the measured reflectivity, it is usually necessary to produce a model of the interface and fit the model parameters to the reflectivity. This procedure does not necessarily lead to a unique solution of the reflectivity profile, as several models may produce identical fits. (This problem is well appreciated in ellipsometry, the optical analogue of our approach.) One advantage of the neutron methodology is the use of contrast variation, which places a constraint on the model; by changing the isotopic contrast (usually H for D) of a film or solvent species in the system, the reflectivity is changed without changing the structure of the system. Thus all the measured reflectivity profiles must be fit by the same structural model.

Model independent information can also be obtained from the reflectivity profile. First, total reflection of neutrons occurs below a critical value of Q, Q_c, related to the change in scattering length density, $\Delta(Nb)$, at the interface by

$$Q_c = [16\pi\Delta(Nb)]^{1/2} \qquad (2)$$

Thus determination of the critical edge, when present, allows determination of the interfacial scattering length density change. Second, the layer thickness, d, can be calculated from the Q spacing of the interference fringes, Q, which arise from reflection from the interfaces of a layer ($d = 2\pi/\Delta Q$). Finally, the amplitude of the fringes in a reflectivity profile depends on the change in scattering length density across an interface; damping of these fringes signals diffuseness of the interface.

We have used neutron reflectivity to study electroactive Pd/polybithiophene interfaces.[15,16] That work indicated formation of a dense polymer film next to the Pd electrode, becoming very diffuse as one moves out toward the solution. This sort of structural information is very useful to the electrochemist, as not only the electron transfer but also the solvent and ion transport determine the performance of an electrochemical system. Here, neutron reflectivity is used to elucidate the structure of the two electroactive polymer bilayer systems, polybithiophene/polypyrrole (PBT/PPy) and polybithiophene/polyxylylviologen (PBT/PXV), to show the difference in structure resulting from the different fabrication routes. Reflectivity from two-component nonelectroactive polymer systems has previously been addressed for spin cast films[21,22] to show polymer motion as a result of thermally driven interdiffusion. Our objective here is to make in situ reflectivity measurements on "buried" electroactive polymer interfaces maintained under electrochemical control and to determine the property−structure correlations which result from different fabrication methods. Previous work[15,16] on PBT single films provided a starting point for the present bilayer studies.

To illustrate the approach, consider the scattering length density profile, $Nb(z)$, of a two-component polymer layer (containing no solvent). It will depend on the spatially variant volume fractions of each polymer, $\phi_A(z)$ and $\phi_B(z)$, and their

(15) Roser, S. J.; Richardson, R. M.; Swann, M. J.; Hillman, A. R. *Faraday Trans.* **1991**, *87*, 2863.
(16) Richardson, R. M.; Swann, M. J.; Hillman, A. R.; Roser, S. J. *Faraday Discuss.* **1992**, *94*, 295.
(17) Penfold, J.; Thomas, R. K. *J. Phys.: Condens. Matter* **1990**, *2*, 1369.
(18) Russell, T. P. *Mater. Sci. Rep.* **1990**, *5*, 171.
(19) Bland, J. A. C. In *Magnetism of Ultrathin Magnetic Structures*; Bland, J. A. C., Heinrich, B., Eds.; Springer-Verlag: Berlin, 1994; p 305.
(20) Penfold, J.; Richardson, R. M.; Zarbakhsh, A.; Webster, J. R. P.; Bucknall, D. G.; Rennie, A. R.; Jones, R. A. L.; Cosgrove, T.; Thomas, R. K.; Higgins, J. S.; Fletcher, P. D. I.; Dickinson, E.; Roser, S. J.; McLure, I. A.; Hillman, A. R.; Richards, R. W.; Staples, E. J.; Burgess, A. N.; Simister, E. A.; White, J. W. *Faraday Trans.* **1997**, *93*, 3899.
(21) Fernandez, M. L.; Higgins, J. S.; Penfold, J.; Ward, R. C.; Shackleton, C.; Walsh, D. J. *Polymer* **1989**, *29*, 1923.
(22) Fernandez, M. L.; Higgins, J. S.; Penfold, J.; Shackleton, C.; Walsh, D. J. *Polymer* **1990**, *31*, 2146.

scattering length densities, Nb_A and Nb_B, according to

$$Nb(z) = \phi_A(z)Nb_A + [1 - \phi_A(z)]Nb_B \quad (3)$$

where $[\phi_A(z) + \phi_B(z)] = 1$. In the electrochemical context, the presence of solvent and/or electrolyte species will be associated with additional *Nb* terms in eq 3. This permits the distributions of the polymers at the electrochemical interface to be determined.

Experimental Section

Neutron Electrochemical Cell. The neutron electrochemical cell[15,16] consisted of the working electrode (forming the top of a box), a Teflon spacer (forming the walls) containing ports for solvent inlet/outlet and for counter and reference electrodes, and a glass block (as the base of the box). The working electrode consisted of an evaporated thin metal film (Pd or Au) on an optically polished single-crystal quartz block (Gooch and Housego Ltd.) of dimensions 100 × 50 × 10 mm. Quartz was used for its high transmission of neutrons, ca. 70% for the 10-cm length. The effective area of the working electrode, as defined by the walls of the Teflon cell, was 30 cm^2 for the PBT/PXV work and 25.5 cm^2 for the PBT/PPy work. The counter electrode located next to the glass block was Pt gauze. The reference electrode was Ag^+ (0.1 mol dm^{-3})/Ag^0 in acetonitrile, isolated from the cell by a Vycor frit; separate measurements showed the Ag^+/Ag^0 reference electrode to be 0.25 V vs SCE, relative to which all potentials are quoted. Potentials were controlled and currents measured using a Thompson Electrochem potentiostat. All solutions were purged with Ar before use for electrochemistry.

Chemicals. 2,2′-Bithiophene, tetraethylammonium tetrafluoroborate (TEAT) (both from Aldrich), and tetraethylammonium hexafluorophosphate (TEAPF) (Fluka) were used as received. Acetonitrile was dried over calcium hydride and then distilled. Pyrrole was purified by distillation. Polyxylylviologen (PXV) was formed by the condensation of equimolar amounts of 4,4′-dipyridyl and α,α′-dibromoxylene in dry acetonitrile.[23] The resulting dibromide salt of the PXV^{2+} ion was recrystallized from an aqueous ammonium hexafluorophosphate solution to yield $PXV(PF_6)_2$.

Electrode Fabrication. The working electrode consisted of a 350 nm thick layer of either Pd or Au. For different experiments, underlayers of either Nichrome (90:10) or 3-mercapto(propyl)trimethoxysilane (Aldrich) were used to improve electrode adhesion to the quartz. The quartz block was prepared for coating with the thiol by an initial 1-h soak in 9:1 H_2SO_4/H_2O_2 at 90 °C. *Caution: This solution reacts violently with many organic materials.* The block was then rinsed with pure water and dried well. It was then transferred to a solution of 10 g of water and 10 g of the thiol in 400 mL of 2-propanol and refluxed for 10 min. The block was then rinsed off and dried in an oven at 108 °C, ensuring that the temperature did not exceed 115 °C. These last steps were repeated three times to ensure complete coverage of the quartz block.

The inner layer, PBT (see Scheme 1 for chemical structures), was deposited by potentiodynamic electropolymerization (scan rate of 20 mV s^{-1}) from a solution containing 10−30 mmol dm^{-3} 2,2′-bithiophene dissolved in 0.1 mol dm^{-3} TEAT/acetonitrile. Polymer coverage was controlled via the anodic potential limit (1.20−1.25 V) and the number of potential cycles (6−13). The outer layer of PPy was formed through electropolymerization of 0.1 mol dm^{-3} pyrrole, in a 0.1 mol dm^{-3} TEAT/acetonitrile solution, by a potential step from 0.0 to 0.9 V vs SCE. The outer layer of PXV was formed through electroprecipitation of the preformed polymer. The following procedure was carried out in a glovebag under nitrogen or argon. First the $PXV(PF_6)_2$ salt in a 0.1 mol dm^{-3} tetraethylammonium hexafluorophosate (TEAPF)/acetonitrile solution was electroreduced to the PVX^+ ion at −0.7 V vs SCE. When the current had fallen to less than 1% of the original value, the purple PXV^+ solution was transferred into the electrochemical cell containing the PBT layer which had been rinsed with acetonitrile to remove monomer and electrolyte. The potential was then swept from 0 to −2.0 V and then back to −1.8 V, where the potential was held for 2 min to increase the film thickness. The electrochemical cell was then electrically isolated and the PXV^+ solution rinsed out with acetonitrile, followed by a 0.1 mol dm^{-3} tetraethylammonium perchlorate (TEAP)/acetonitrile solution, since the perchlorate salt of PXV^{2+} was found to be insoluble.

Scheme 1. Monomer and Polymer Structures for (A) Pyrrole/Polypyrrole, (B) Bithiophene/Polybithiophene, and (C) Polyxylylviologen

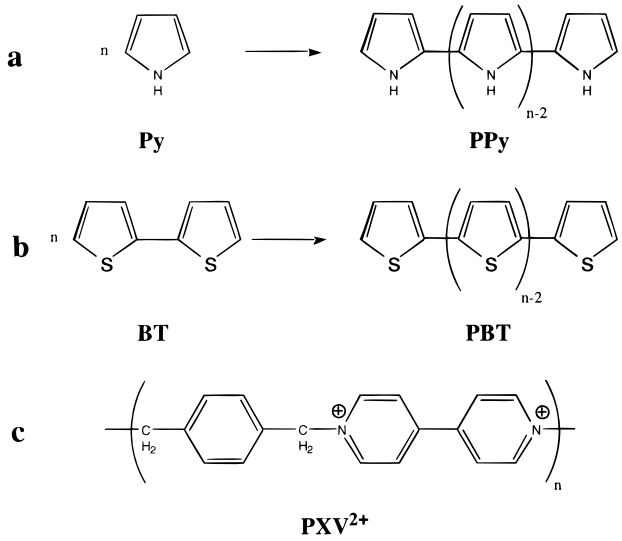

Neutron Instrumentation. Reflectivity measurements were made using the CRISP time-of-flight neutron reflectometer at the ISIS Facility, Rutherford Appleton Laboratory, Oxford. Measurements were made either with a multidetector at an incident angle of 0.4° and over a wavelength range of 0.1−1.04 nm or with a single detector at incident angles of 0.35°, 0.8°, and 1.8° and a wavelength range of 0.05−0.64 nm. The former provided a momentum transfer range from 0.08 to 0.8 nm^{-1} and the latter a range from 0.1 to 3 nm^{-1}, well down into the background levels of the system. Collimation slits were varied to ensure constant illuminated length of the sample and constant resolution. These parameters ensured that all of the film thickness and about 80% of the electrode area were sampled; thus, there is no ambiguity about representative sampling of the interface. Run times depended on the contrast of the system, but typically required 2−3 h to cover the three angles. Reflectivity profiles were corrected for transmission through the quartz block and then put on an absolute scale by dividing the transmission-corrected reflectivity by the intensity at long wavelengths for transmission through air.

Calculated values for the scattering length densities of the various components of the electrochemical system are presented in Table 1. For the PBT/PPy bilayer, reflectivity measurements were made on films fabricated with pyrrole, h-Py, and perdeuterated pyrrole, d-Py. The use of deuteration was to enhance the contrast between the PBT and PPy portions of the film which would otherwise have very similar scattering length densities. Solvent contrasts used were acetonitrile, CH_3CN, and quartz contrast matched acetonitrile, QCMA (a case where CH_3CN and CD_3CN are mixed in a ratio of 21:79 (v/v) so that the resulting scattering length density is that of quartz). Uncertainties in the fitted thickness and scattering length density are estimated to be about ±1 nm and ±0.2 × 10^{10} cm^{-2} for a particular model based on the scatter in the parameters which produced equally good fits. In modeling[17,24,25] the electrochemical interface, reflectivity measurements made during each step of electrode fabrication are fitted so that a comprehensive picture was developed. This involved measurements of the bare electrode and then as each layer of electroactive material was added in, using as many

(23) Factor, A.; Heinsohn, G. E. *J. Polym. Sci., Polym. Lett.* **1971**, *9*, 289.

(24) Sivia, D. S.; Hamilton, W. A.; Smith, G. S. *Physica, B* **1991**, *173*, 121.

(25) Penfold, J. In *Neutron, X-ray and Light Scattering*; Lidner, P., Zemb, Th., Eds.; Elsevier Science: Amsterdam, 1991; p 223.

Table 1. Calculated Values for the Scattering Length Densities of Components in the Electrochemical Cell

material	MW (g mol^{-1})	$\sum b_i$ (10^{-12} cm)	ρ (g cm^{-3})	Nb[a] (10^{10} cm^{-2})
quartz	60.09	1.575	2.63	4.15
Pd	106.4	0.60	12.02	4.07
Au	196.97	0.76	19.3	4.48
CH_3CN	41.05	0.483	0.786	1.32
CD_3CN	44.08	3.606	0.844	4.90
PBT	164.24	4.38	1.21	1.94
PPy	65.02	2.48	1.0	2.30
$(PPy)_3(BF_4)$	281.87	10.21	1.0	2.18
d-PPy	68.04	5.60	1.0	4.95
$(d\text{-}PPy)_3(BF_4)$	290.93	19.57	1.0	4.05
$PXV(ClO_4)_2$	458.94	14.43	1.0	1.89
$d\text{-}PXV(ClO_4)_2$	475.14	31.08	1.0	3.94

[a] Where precise polymer densities are unknown, the uncertainties are <10%; these translate to uncertainties in scattering length density of <10%.

contrasts as possible. Where a Nichrome bonding underlayer was used (see Electrode Fabrication), this was incorporated in the model. When fitting the reflectivity profile of the next added layer, the fitted parameters of the previous step are used as a starting point and initially fixed. If these parameters had changed and the quality of fit, χ^2, did not improve, then the parameters were allowed to float. (This strategy places a constraint on the fitting.) The model which was chosen to represent the film structure was selected on the basis of the lowest χ^2 (typically on the order of 1−3) and best visible fit to the reflectivity. Where several models of varying film thickness produced similar fits and χ^2 values, electrochemical information was used to identify the physically meaningful solution.

Results and Discussion

Part 1. Reflectivity and Structure of Polybithiophene Films. PBT film structure has previously been characterized using neutron reflectivity.[15,16] However, it is necessary to refine this further as the starting point for defining the "bilayer" structures. In the first stage of bilayer fabrication, a PBT film was electropolymerized onto the metal electrode; a typical cyclic voltammogram for the polymerization is shown in Figure 1. An estimate of the minimum surface coverage can be obtained from the integrated current in the polybithiophene reduction peak. This procedure assumes that the film was completely oxidized and reduced on the time scale of the experiment, i.e., there is no charge trapping;[26] previous electrochemical data[10,11,12] for these systems support this assertion. Various electrochemical and neutron parameters for the films studied in this paper are presented in Table 2. Three films, designated PBT1, PBT2, and PBT3, were polymerized by 6, 6, and 13 cycles about the potential limits 0 to 1.20, 1.23, and 1.25 V, giving charge-based coverages of 11.5, 13.8, and 30 nequiv cm^{-2}, respectively (1 nequiv represents 10^{-9} mol of electronic charge). Neutron reflectivity was used to study these films, as described below.

Previous neutron reflectivity measurements[15,16] showed that PBT films are fairly compact at the metal interface and become more diffuse as one moves out into solution. This is a result of potential cycling during polymerization, allowing monomer to diffuse into the structure of the PBT film and then undergo polymerization on the next cycle. Figure 2a shows reflectivity profiles and fits for the three PBT films. To remove the Q^{-4} effect (see eq 1), reflectivity data are plotted in RQ^4 vs Q format; this allows highly critical assessment of data fitting quality. Small fringes of spacing $\Delta Q = 0.018$ nm^{-1}, visible at low values of Q, result from reflection of neutrons from the interfaces of the metal electrode, which is ca. 350 nm thick. A minimum in the reflectivity from film PBT1, at a momentum transfer of 0.2 nm^{-1}, results from interference from the neutron reflection off the two polymer interfaces (metal/polymer and polymer/solution). The polymer/solution interfaces for the other two films are more diffuse, as demonstrated by the absence of a clear minimum in the RQ^4 vs Q plots of Figure 2a.

Figure 2b shows the best fit scattering length density profiles resulting from the modeling procedure as a function of film thickness; parameters are presented in Table 2. The model used to fit the reflectivity profiles was essentially that of a single slab consisting of the polymer film (quartz/PBT/QCMA). This model works due to the closeness in the scattering length densities of the quartz and Pd electrode. For very good fits a two-slab model incorporating the 350-nm metal electrode and the polybithiophene layer produced a better result (quartz/Pd/PBT/QCMA). In the case of film PBT2, a three-slab model (quartz/Pd/PBT2a/PBT2b/QCMA) was found to improve the fit. The diffuseness of the polymer/solution interfaces is represented by the roughness parameter, r, and is responsible for the small amplitude of the fringes. Results of these fitting procedures are summarized in Table 2.

Using the model parameters for the film thickness and scattering length density, polymer and solvent volume fraction profiles can be calculated for these PBT films (assuming a scattering length density of 2.1×10^{10} cm^{-2} for bulk PBT[15,16]). The outcome is shown in Figure 3. The films show appreciable variations (see below) in solvent content in the film adjacent to the electrode surface. The fitted parameters can also be used to calculate the film coverage, Γ_{PBT} ($\Gamma_{PBT} = \phi_p \rho d/\mathrm{MW}$, where ϕ_p is the polymer volume fraction, ρ the bulk polymer density, d the film thickness, and MW the molecular weight of the repeat unit; see Table 2). The mean extent of charge delocalization is then the ratio of the moles of thiophene units present, as seen by the neutrons, to the moles of charge required to reduce (or "undope") the film. For example, this gives a value of 3.3 for PBT2, within the range 3−5 reported in the literature.[27,28] Films PBT1 and PBT3 gave lower ratios, possibly due to leaching out of short chains when the polymerization solution was exchanged for background electrolyte.

In each case, the qualitative PBT film structure is similar: dense at the electrode and diffuse at the solution interface, in agreement with previous findings.[15,16] Other models, notably those where the *dense* → *diffuse* structure is reversed, produced poor fits. A new observation is the effect on film density of the maximum potential to which the electrode was subjected during polymerization. Film PBT2 was obtained by cycling the potential to 1.23 V, whereas PBT1 was only polymerized to 1.20 V. This resulted in a larger film thickness (43 vs 26 nm) and a greater roughness (19 vs 9 nm). More dramatic evidence of this effect is seen in Figure 3c for film PBT3, which was cycled 13 times to 1.25 V. The solvent volume fraction for this film was found to be 0.56, and the surface coverage 30 nmol cm^{-2}, based on the reduction current, and 39 nmol cm^{-2}, based on reflectivity measurements. These results clearly show the effect of higher potential limits during polymerization on the polymer structure and may indicate the origin of reported differences in nominally similar materials produced by different electropolymerization protocols.[27,28]

Part 2. Reflectivity and Structure of Polybithiophene/Polypyrrole Films. Electropolymerization of pyrrole after

(26) Bandey, H. L.; Cremins, P.; Garner, S. E.; Hillman, A. R.; Raynor, J. B.; Workman, A. D. *J. Electrochem. Soc.* **1995**, *142*, 2111.

(27) *Handbook of Conducting Polymers*, Skotheim, T. A., Ed.; Marcel Dekker: New York, 1986.

(28) Roncali, J. *Chem Rev.* **1992**, *92*, 711.

Table 2. Best-Fit Parameters to Reflectivity Profiles of the PBT, PBT/PPy, and PBT/PXV Films

film and solution	layer	E_{upper} (V (SCE))	d (nm)	Nb (10^{10} cm^{-2})	r (nm)	Γ_q[a] (nequiv cm^{-2})	Γ_N[b] (nmol of thiophene cm^{-2})	ϕ_P
Pd/PBT1/QCMA	1	1.20	26	2.6	8.5	11.5	14	0.75
Pd/PBT2/QCMA	1	1.23	43	2.5	4.3	13.8	46	0.75
	2		17	2.7	18.8			
Pd/PBT3/QCMA	1	1.25	60	3.1	16.9	30	39	0.44
Au/PBT4/QCMA	1	1.20	46	2.1	12.6	20	62	0.91
Pd/PBT1/d-PPy/QCMA	1		16	3.1	1.9			
	2		10	3.5	6.8			
Pd/PBT1/d-PPy+d-PPy/QCMA	1		14	3.0	10.5			
Pd/PBT2/h-PPy/QCMA	1		42	2.6	17.2			0.75−0.85
	2		16	2.8	20.4			
Pd/PBT3/d-PPy/QCMA	1		54	3.3	17.5			
Au/PBT4/d-PXV/QCMA	1		43	2.3	15.6	17[c]		
Au/PBT4/d-+XV/CH_3CN	1		45	1.9	8.4			
	2		27	2.7	10.0			

[a] Surface coverage based on integrated charge in oxidation peak. [b] Surface coverage based on scattering length density and film thickness. [c] Surface coverage based on conversion of PXV^{2+} to PXV^0.

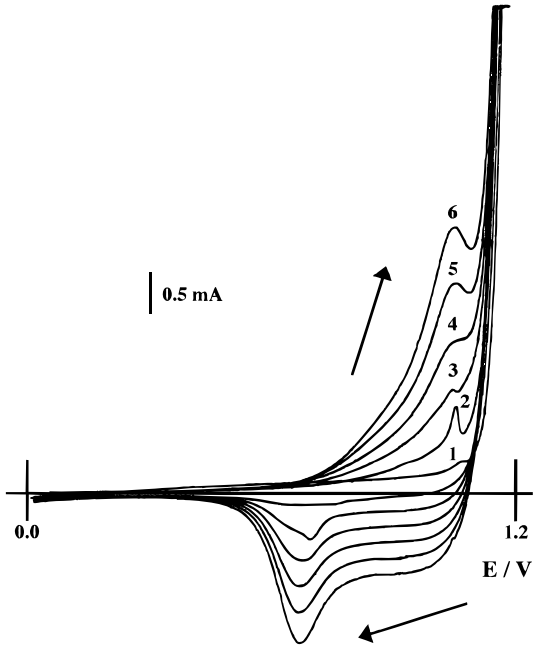

Figure 1. Cyclic voltammogram for the electrodeposition of a PBT film from 0.1 mol dm^{-3} bithiophene in acetonitrile with 0.1 mol dm^{-3} TEAT as the supporting electrolyte. Potential limits: 0.0−1.20 V. Scan rate: 20 mV s^{-1}. Arrows indicate the scan direction, and numbers indicate cycle number.

formation of the PBT1 film was accomplished by stepping the electrode potential to 0.9 V (vs SCE) in an acetonitrile solution containing 0.1 mol dm^{-3} pyrrole and 0.1 mol dm^{-3} TEAT. Polymerization was terminated by stepping the potential back to 0.0 V. A cyclic voltammogram of the resulting PBT1/PPy film formed in this manner is shown in Figure 4. The electrochemical oxidation and reduction of the outer layer in a perfect bilayer is mediated by the electrochemistry of the inner layer.[4] For this film, current flow due to the oxidation and reduction of polypyrrole is observed at potentials characteristic of polypyrrole single film electrochemistry. As discussed previously[10,11] this is indicative of "outer" layer penetration to the underlying metal electrode.

Figure 5a shows the change in the reflectivity after each addition of d-PPy, with the corresponding fits. In this case perdeuterated pyrrole was used to provide maximum contrast between depositting PPy and previously deposited PBT (d-PPy looks more like the solvent than the previously deposited PBT). The model used to fit the reflectivity for the initial addition of

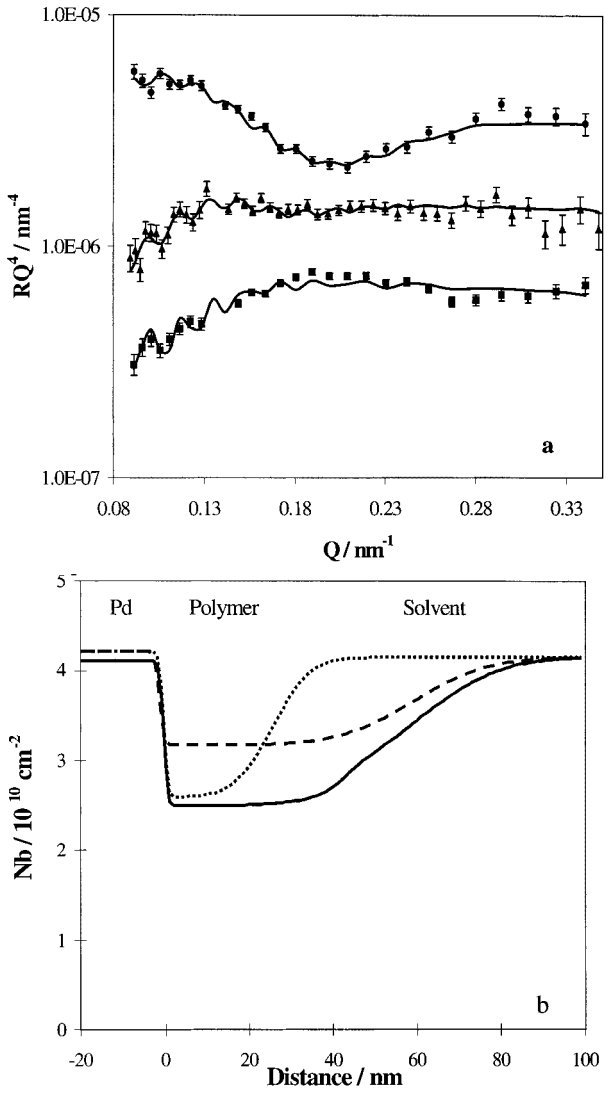

Figure 2. (a) Reflectivity profiles (markers) and fits (lines) for the films PBT1 (●), PBT2 (■), and PBT3 (▲). The electrode arrangement is quartz/Pd/PBT/QCMA with the neutrons entering through the quartz. For presentational clarity, the reflectivity profile for film PBT2 is offset downward by a factor of 0.5. (b) Scattering length density profiles for PBT1 (solid line), PBT2 (dotted line), and PBT3 (dashed line).

d-PPy consisted of the Pd electrode and two polymer layers. The overall polymer thickness did not change, but division of

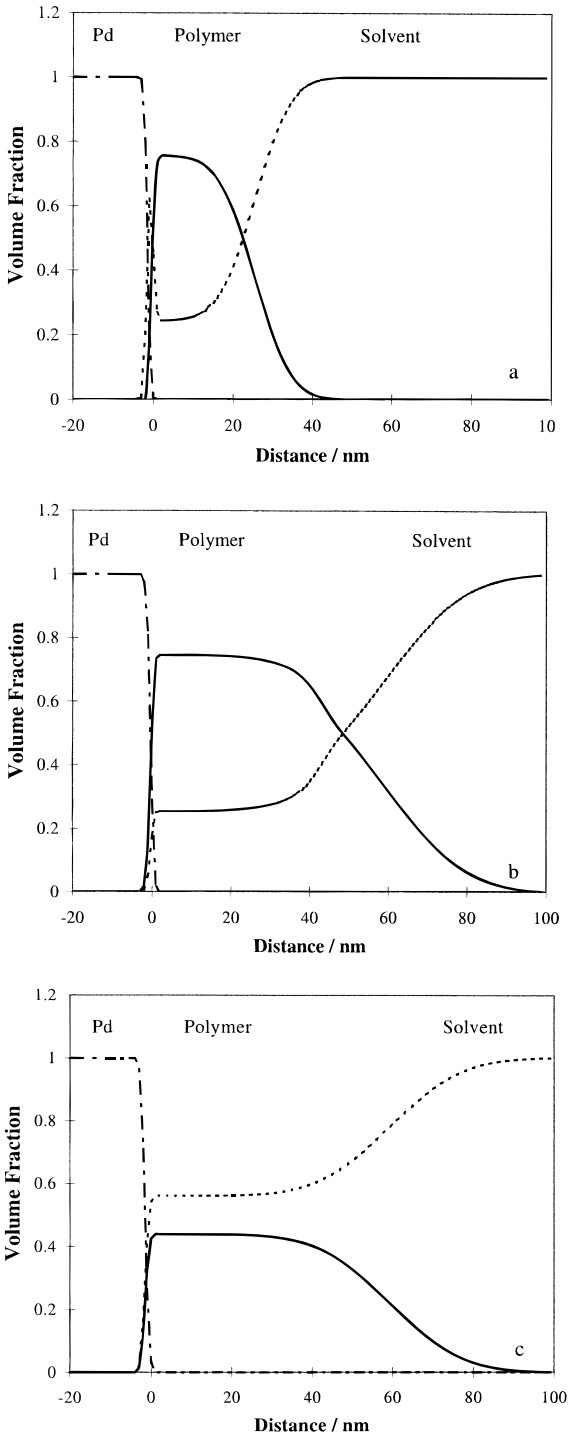

Figure 3. Volume fraction profiles for films (a) PBT1, (b) PBT2, and (c) PBT3 polymerized at 1.20, 1.23, and 1.25 V, respectively. The Pd electrode is represented by the dot-dashed line, the PBT film by the solid line, and the solvent by the dashed line.

the original layer into two produced a better fit. The fringe in the reflectivity from the PBT interfaces is not as evident as for the PBT1/PPy film, indicating an increase in the scattering length density of the polymer layer and/or an increase in the diffuseness of the film. In either case, this results in decreased contrast between the film and the solution. Thus, as seen in Figure 5b, a second addition of d-PPy to the PBT1/d-PPy film resulted in further reduction of the fringe intensity. A single layer was then used to represent the polymer; more complex models did not produce a better fit, i.e., the two-component system behaved as a composite.

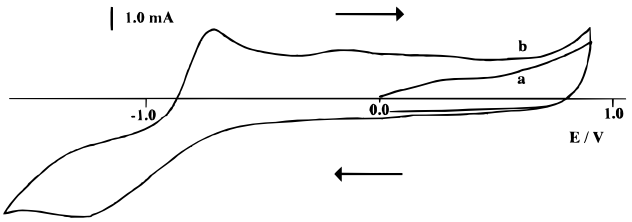

Figure 4. Cyclic voltammogram for PBT1/PPy film in an acetonitrile solution containing 0.1 mol dm^{-3} TEAT. Scan rate: 20 mV s^{-1}. Arrows indicate scan direction; "a" and "b" indicate the first and second cycles, respectively.

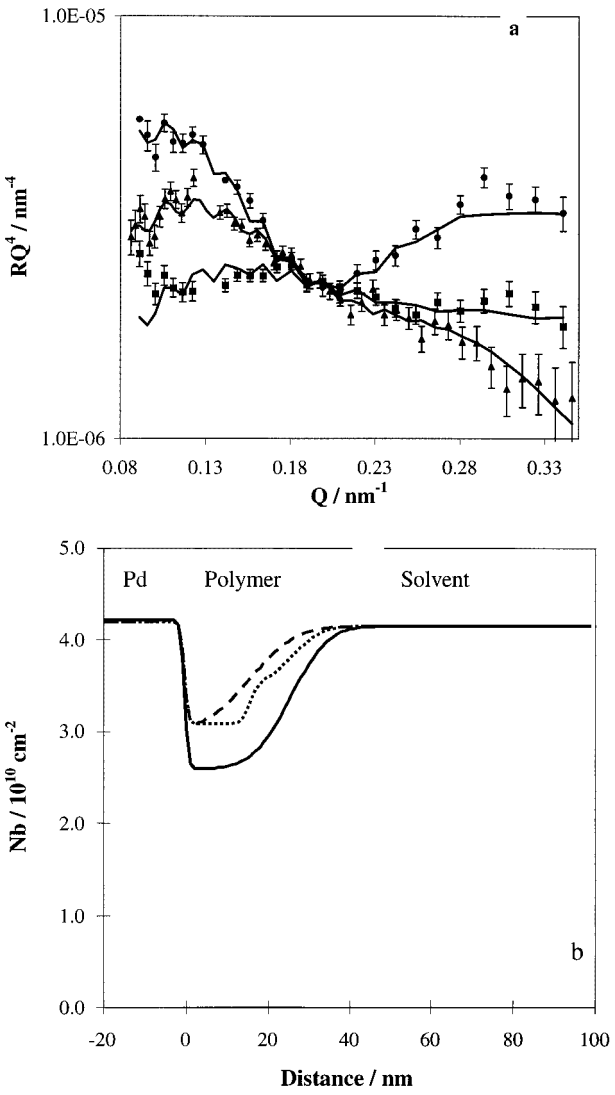

Figure 5. (a) Reflectivity profiles (markers) and fits (lines) for the films PBT1 (●), PBT1/d-PPy (▲), and PBT1/d-PPy+d-PPy (■). The cell configuration is quartz/Pd/polymer/QCMA with 0.1 mol dm^{-3} TEAT in the acetonitrile. (b) Scattering length density profiles show the changes which occur to the PBT1 film (full line) as the composite structure PBT1/d-PPy (dotted line) is formed. Further addition of d-PPy (dashed line) reduces the contrast between the composite and solvent.

The profiles in Figure 5b show a progressive increase in the scattering length density of the PBT layer as d-PPy is added to the film. This observation is consistent with incorporation of deuterated polypyrrole in the PBT matrix. The scattering length density of the composite film is larger than would be expected if the deuterated pyrrole simply replaced the solvent which existed in the film. This indicates a swelling of the PBT layer through inclusion of extra solvent and polypyrrole. However,

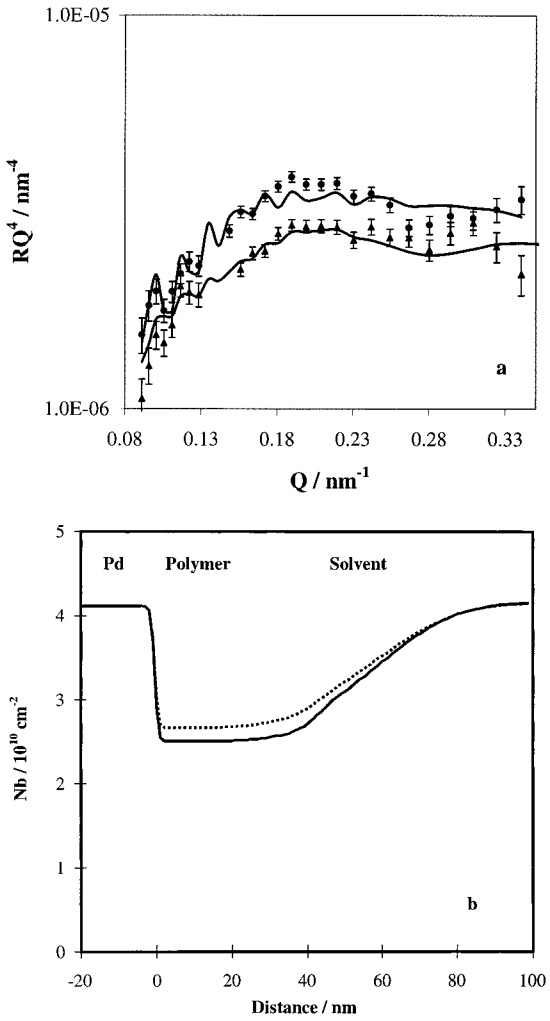

Figure 6. (a) Reflectivity profiles (markers) and fits (lines) for the films PBT2 (●) and PBT2/h-PPy (■). The electrode arrangement is quartz/Pd/polymer/QCMA with 0.1 mol dm^{-3} TEAT in the acetonitrile. (b) Scattering length density profiles show the small changes which occur to the PBT2 film (full line) as the composite structure PBT2/h-PPy (dotted line) is formed.

the scattering length density profile of the bilayer appears to extend over a shorter distance than the PBT layer. This is an artifact due to the lack in contrast between the solvent and deuterated pyrrole, which makes it *appear* that the polymer film is thinner. Similar results were observed when more d-PPy was added to the PBT1/d-PPy film.

Although well suited to demonstrating that PPy penetrates into the PBT layer, the use of deuterated pyrrole is not the best option for directly observing the formation of polypyrrole itself at the solution interface of the PBT film. This is due to the similar contrast of d-PPy with QCMA. Hydrogenous polypyrrole, h-PPy, which contrasts strongly with the QCMA solvent, is a better choice for this purpose. It should show up as an extension to the film thickness, with a slight increase in the scattering length density of the layer. Figure 6a shows the reflectivity profiles with fits for PBT2 and PBT2/h-PPy films against QCMA. The scattering length density profiles from the best fit parameters are presented in Figure 6b. As predicted there is an increase in the scattering length density of the polymer layer, which is again larger than expected. The composite film is calculated to hold between 15 and 25% solvent (based on the polymer being completely h-PPy or completely PBT). However, the data of Figure 6 provide no such evidence of a

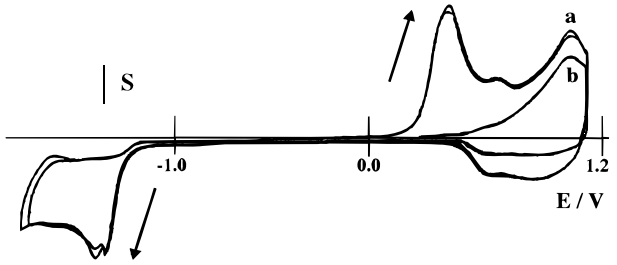

Figure 7. Cyclic voltammogram of the PBT/PXV bilayer in 0.1 mol dm^{-3} TEAP: (a) potential cycled between −1.8 and 1.1 V, (b) potential cycled between 0.0 and 1.1 V after the outer layer was trapped in its oxidized state. Scan rate: 20 mV s^{-1}. Current sensitivity: (a) $S = 2$ mA, (b) $S = 5$ mA.

discontinuity in the scattering length density profile. In the event that the PPy were deposited in a separate layer at the PBT/solvent interface, i.e. the film were a bilayer, one would have found a discontinuity in composition. The conclusion is that PBT,PPy is a composite film.

Failure to form a bilayer in the case of PBT,PPy is a consequence of the method used to form the outer layer. As shown in the previous section, the solvent volume fraction in the interior of film PBT1 was 0.25. This allowed penetration to the metal electrode of pyrrole monomer which, on polymerization, formed a composite film. The composite structure allows the polypyrrole to be oxidized or reduced independently of the PBT, by direct electronic communication with the underlying electrode.

Part 3. Reflectivity and Structure of Polybithiophene/Polyxylylviologen Films. For this bilayer the PBT film was electropolymerized as above, using 12 cycles up to a potential of 1.20 V. The preformed polymer polyxylylviologen was electroprecipitated onto the PBT film. The cyclic voltammogram of the PBT4/PXV bilayer is shown in Figure 7: its form suggests that a good bilayer has been fabricated. A detailed exposition of the purely electrochemical response has been given elsewhere,[10−13] but we summarize the key features in order to set the scene for the new structural data we present here. The oxidation waves at 0.4 and 1.0 V are due to the oxidation of the $PXV^{0/2+}$ and $PBT^{0/1+}$ layers, respectively. Reduction waves at about 0.8 and −1.4 V correspond to the $PBT^{1+/0}$ and $PBT^{0/1-}$/$PXV^{2+/0}$ layers, respectively. Oxidation of the PXV layer occurs immediately a conducting path is formed through the PBT layer, so it *appears* that the PXV is oxidized before the PBT. This cyclic voltammogram shows "classic" bilayer response: rectifying characteristics with charge trapping/untrapping features. We note the absence of current passage for potentials in the range $-1.0 < E/V < 0.0$, i.e. where the $PXV^{2+/1+}$ and $PXV^{1+/0}$ redox potentials lie. Trace "a" corresponds to a full potential cycle between −1.8 and 1.1 V. This shows the oxidation of the outer $PXV^{0/2+}$ layer at 0.4 V and its subsequent reduction at −1.35 V ($PXV^{2+/0}$). The potentials at which polybithiophene is oxidized and reduced represent very large overpotentials for driving viologen redox chemistry. Thus formation of a conducting path through the PBT layer leads to rapid electron transfer with the outer layer. The current peak at 1.05 V results from the oxidation of the PBT. Trace "b" was recorded by sweeping the potential between 0 and 1.1 V after initially oxidizing the bilayer (note the scale change between scans "a" and "b"). The charge passed in this cycle represents the charge required to oxidize and reduce the PBT "inner" layer alone. An estimate of the PXV coverage is then $\Gamma_{PXV} = 17$ nequiv cm^{-2}. The initial

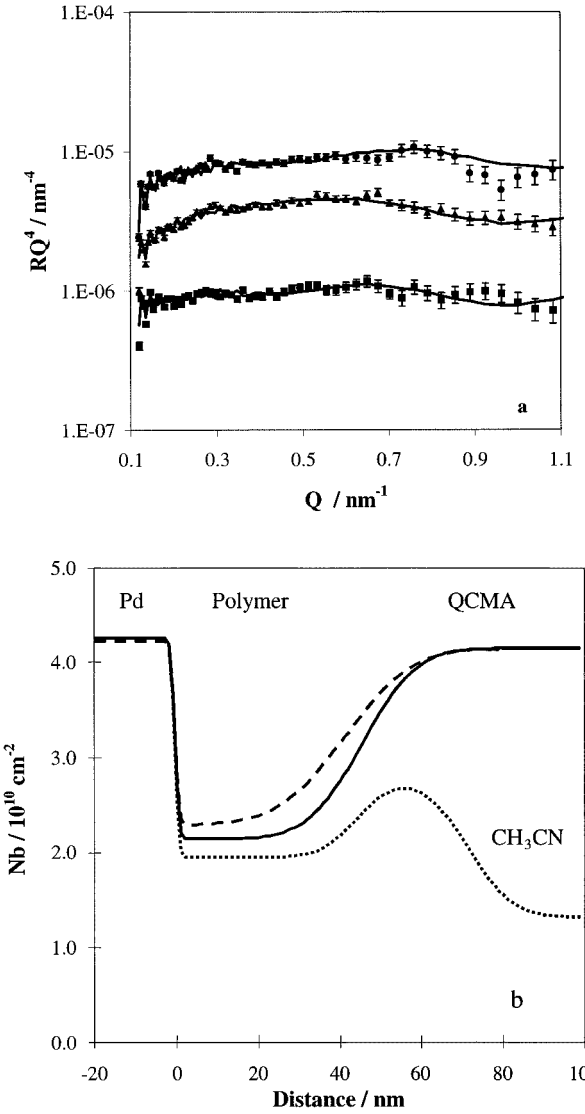

Figure 8. (a) Reflectivity profiles (markers) and fits (lines) for the films quartz/Au/PBT/QCMA (●), quartz/Au/PBT/d-PXV/QCMA (▲), and quartz/Au/PBT/d-PXV/CH_3CN (■). For presentational clarity, the latter two profiles are offset downward by factors of 0.5 and 0.1, respectively. (b) Scattering length density profiles for interfacial structures quartz/Au/PBT/QCMA (solid line), quartz/Au/PBT/d-PXV/QCMA (dashed line), and quartz/Au/PBT/d-PXV/CH_3CN (dotted line).

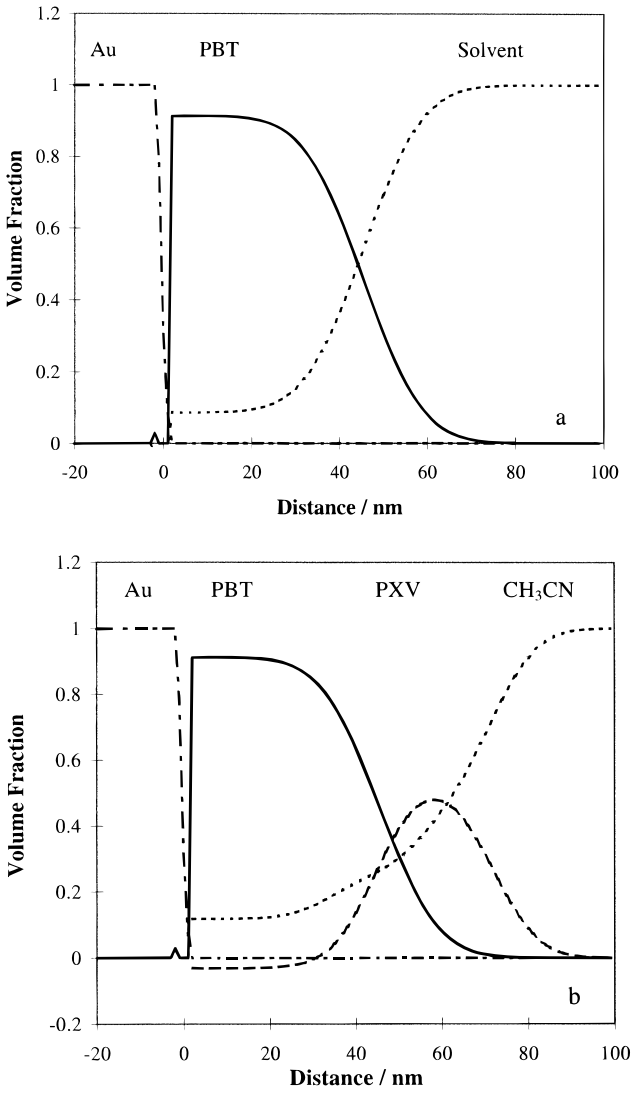

Figure 9. Volume fraction profiles for (a) PBT4 and (b) PBT4/d-PXV. The Au electrode is represented by the dot-dashed line, PBT by the solid line, d-PXV by the dashed line, and the solvent by the dotted line.

charge-based coverage of PBT from the deposition process was $\Gamma_{PBT} = 20$ nequiv cm^{-2}, and from the bilayer, it was 21 nequiv cm^{-2}.

The reflectivity profiles and fits shown in Figure 8a are for the films Au/PBT4/QCMA, Au/PBT4/d-PXV/QCMA, and Au/PBT4/d-PXV/CH_3CN. (The latter two profiles are offset downward by factors of 0.5 and 0.1, respectively, for presentational clarity.) The model used to fit the reflectivity of the PBT film consisted of three layers; the Nichrome underlayer between the Au and quartz, the Au electrode and the polymer. For the bilayer reflectivity profiles, another layer was required to fit the film against CH_3CN, while against QCMA, the lack of contrast between deuterated PXV and the solvent necessitated only a three-layer model.

Figure 8b shows the scattering length density profiles for this bilayer. The data underline the power of the contrast variation technique (cf. QCMA and CH_3CN profiles), in this case, in locating the position of the PXV component. The polybithiophene layer (solid line) was polymerized by 12 cycles up to a potential of 1.20 V. This produced a dense film with a solvent volume fraction, at the Au/PBT interface, of 0.09. The fitted film roughness is intermediate between those found for films PBT1 and PBT2. The surface coverage of this polymer layer, based on the charge in the reduction peak of the PBT film, is 20 nequiv cm^{-2}, nearly twice that obtained for PBT1, which was polymerized using only six cycles. From the best-fit parameters, a neutron-based coverage of $\Gamma_{PBT} = 62$ nmol cm^{-2} was calculated, giving a ratio of 3.1 thiophene units per charge unit. The electroprecipitation of d-PXV, which has a scattering length density very close to that of quartz, produces the bilayer whose structure is best seen against CH_3CN (dotted line). Against QCMA (dashed line) the outer layer is effectively contrasted out. A change is noted in the scattering length density of the PBT region of the film ($0 \leq z/\text{nm} \leq 20$) after the PXV layer was added, indicative of a slightly larger solvent volume fraction.

The volume fraction profiles for the original PBT film and the bilayer system are shown in Figure 9. As mentioned above, there is very little solvent at the metal/PBT interface, as a consequence of the low maximum potential to which the film was cycled during polymerization (i.e., the slow deposition rate) and the large number of deposition cycles (Figure 9a). This

initial profile for the PBT was then used to create a volume fraction profile for the PBT/PXV bilayer (Figure 9b) on the basis that the PBT layer did not change. We know this is only an approximation from the difference in the scattering length density profiles and the apparent negative volume fraction found for the PXV (dashed line); we estimate the associated uncertainties in volume fractions to be <5%. Nevertheless, given the complexity of the structural problem and the fact that we have dealt with the issue of spatial variations of composition, this is an appreciable achievement. Qualitatively, the primary conclusion is that the outer layer is well separated from the metal electrode by the PBT. Thus electroprecipitation of the preformed polymer PXV leads to a good bilayer, due to the inability of the polyxylylviologen to penetrate through the PBT to the metal electrode. Consequently spatial distribution, i.e., interfacial architecture, is the primary determinant of electrode current−voltage characteristics.

Conclusions

For the purpose of determining in situ structure−property correlations of electroactive films neutron reflectivity has great potential. Quite often electroactive polymer devices fabricated under similar conditions result in films which perform very differently. We have been able to show here that there are systematic variations in solvent volume fractions between films produced under different potential conditions, though the overall structure is qualitatively maintained.

Reflectivity in this study has been used to show the structural consequences of different "bilayer" fabrication methods. Formation of a bilayer by polymerizing pyrrole directly onto a polybithiophene film leads to composite formation, i.e. complete interpenetration of electroactive components. Electroprecipitation of polyxylylviologen onto a polybithiophene film results in segregated layers with a small degree of interpenetration. The different structures produced by these two fabrication methods explain why the two systems have such dramatically different electrochemical responses.

Acknowledgment. We acknowledge funding by the EPSRC (GR/J30516) and thank the ISIS Facility (Rutherford Appleton Laboratories) for beam time on the CRISP reflectometer. We also thank M. Gonsalves, D. Loveday, and A. Zarbakhsh for technical assistance and useful discussions.

JA970301H